fractal and fractional

MDPI

Article

Fractal Characteristics of Geopolymer Mortar Containing Municipal Solid Waste Incineration Fly Ash and Its Correlations to Pore Structure and Strength

Peng Zhang, Xu Han *, Jinjun Guo and Hongsen Zhang

Yellow River Laboratory, Zhengzhou University, Zhengzhou 450001, China
* Correspondence: hanxu@gs.zzu.edu.cn

Abstract: Compression and mercury intrusion porosimetry (MIP) tests were conducted to analyze the effect of municipal solid waste incineration fly ash (MSWIFA) content on the mechanical performance and pore structure of geopolymer mortar. The MSWIFA weight contents were 0%, 5%, 15%, 25%, and 35% and the pore diameter distribution, specific surface area, and pore volume were considered to assess the pore structure of the geopolymer mortars. The popular fractal model was used to investigate the fractal features of the geopolymer mortars. Additionally, mathematical models of fractal dimension with pore structural parameters and compressive strength were established. The results showed that the compressive strength of geopolymer mortars decreased while the total pore volume and total specific surface area of mortars increased with the increase in MSWIFA content. As the MSWIFA content increased, the harmless pores (pore diameter < 20 nm) were refined. Specifically, the pores with a diameter of 5–10 nm increased in number but the pores with a diameter of 10–20 nm decreased in number with the increase in MSWIFA content. The pore structure in the mortars showed scale-dependent fractal characteristics. All fractal curves were divided into four segments according to the pore diameter, namely, Region I (<20 nm), Region II (20–50 nm), Region III (50–200 nm), and Region IV (>200 nm). The surface fractal dimension (D_S) in Region I and Region IV was between 2 and 3. However, the D_S in Region II and Region III was greater than 3, indicating the pores in Region II and Region III were non-physical according to the surface geometry because of the presence of ink bottle pores which distorted the result of the MIP. The complexity of pores in Region I and Region IV was reduced by the addition of MSWIFA. The D_S is a comprehensive parameter that well describes the spatial and morphological distribution of pores in geopolymer mortars and exhibited a good correlation with the specific surface area, pore volume, and compressive strength. A mathematical model based on the D_S was established to predict the compressive strength of the geopolymer mortar containing MSWIFA.

Keywords: municipal solid waste incineration fly ash; geopolymer mortar; compressive strength; pore structure; surface fractal dimension

Citation: Zhang, P.; Han, X.; Guo, J.; Zhang, H. Fractal Characteristics of Geopolymer Mortar Containing Municipal Solid Waste Incineration Fly Ash and Its Correlations to Pore Structure and Strength. *Fractal Fract.* **2022**, *6*, 676. https://doi.org/10.3390/fractalfract6110676

Academic Editors: Zine El Abiddine Fellah, Shengwen Tang and Lei Wang

Received: 16 October 2022
Accepted: 14 November 2022
Published: 15 November 2022

1. Introduction

Cement is widely used the world over as a building material because of its low price and excellent performance. However, its production consumes a lot of energy and causes carbon emissions [1]. It is reported that the energy consumption of cement production accounts for 75% of the entire building materials industry. The production of 1 t cement emits about 1 ton of CO_2 and is listed as one of the main factors causing global warming [2]. Geopolymers are considered environmentally friendly materials with the most potential to replace cement [3,4]. In total, 73% of carbon emissions and 43% of energy consumption can be reduced using geopolymers instead of cement as cementing material [5,6]. Additionally, geopolymer composites exhibit characteristics of early strength, fast hardening, excellent durability, low shrinkage, and high-temperature resistance [7]. Furthermore, geopolymers

show outstanding solidification performance compared to heavy metals due to their special tetrahedral cavity structure. Therefore, geopolymers are the most competitive substitute for cement because of their wide application prospects.

Geopolymers are mainly prepared by alkali activators and aluminosilicate materials (calcined natural minerals or industrial wastes) [8]. Metakaolin (MK), Fly ash (FA), and ground granulated blast furnace slag (GGBFS) are the most commonly used precursors. These three raw materials are also used as mineral admixtures in cement-based composites. Different raw materials reveal their own distinctive characteristics due to various mineral compositions, morphology, and particle size distribution. GGBFS-based geopolymer mortar presents excellent mechanical performance and low preparation temperature requirements, but poor workability resulting from a fast-hardening speed [9,10]. FA-based geopolymer mortar exhibits remarkable workability and durability, whereas its strength development depends on high-temperature curing (60–90 °C). MK-based geopolymer mortar shows prominent mechanical performance and durability, however, it also presents poor workability, large water demand, high reaction heat, and high permeability [11]. Moreover, MK is preferred for preparing geopolymer mortar due to its excellent dispersion in alkaline solutions and easy adjustment of the Si/Al ratio. However, the preparation of MK compared with that of solid wastes leads to extra carbon emissions and energy consumption [12,13]. Therefore, many studies have been conducted on the preparation of geopolymers using solid wastes such as rice husk ash, red mud, slag, and municipal solid waste incineration fly ash (MSWIFA) [14]. These studies thus expand the utilization method of solid wastes.

Power generation by waste incineration is considered the preferred method of municipal solid waste treatment due to the production of green energy and the substantial reduction in waste volume [15]. The bottom ash and MSWIFA are by-products of the waste incineration. The bottom ash is generally considered non-toxic and has been used as an aggregate or admixture because of its high content of silica and aluminum and low content of lithophilic heavy metals such as copper and nickel [16]. However, the MSWIFA needs to be treated because it is rich in heavy metals. Washing, heat processing, and solidification/stabilization (S/S) are the three main methods for MSWIFA treatment [17]. The first two methods are used less often than S/S due to their high cost and complex process. The S/S method encapsulates hazardous substances in the MSWIFA with cementitious materials. Heavy metals will be synthesized as less-toxic compounds or adsorbed on the C-S-H gels when the cement is used for S/S treatment [18]. However, the cement S/S matrix shows poor stability in a long-term environment because the sulfate and chloride salts in the MSWIFA lead to the degradation of the matrix [19]. The use of geopolymers in the S/S treatment of MSWIFA has been widely considered in recent years [20,21]. The three-dimensional amorphous network structure of geopolymers can solidify harmful substances in the MSWIFA because of its strong adsorption and ion exchange performance. In addition, the compact three-position tetrahedral structure of geopolymers can resist chloride ions, resulting in a high stability for the encapsulation of heavy metals [22]. Therefore, geopolymers show broad application prospects in the encapsulation and resource utilization of MSWIFA.

The pore structure obviously affects the physical and mechanical performance and durability of geopolymer mortar [23]. The pores show a wide range of pore diameters, including gel pores, capillary pores, and air bubbles in the mortar. Pores with different pore diameters exhibit various effects on the properties of the mortar [24]. It is generally believed that gel pores affect the shrinkage and creep of mortar but have no effect on the strength. The air bubbles and large capillary pores exhibit an adverse influence on the mechanical properties and durability of mortar but are beneficial to the freeze-thaw resistance [25]. Additionally, the distribution and morphology of pores are disorganized. These characteristics are difficult to describe in the pore structure due to pore volume, pore size distribution, pore surface area, and other parameters. The fractal theory is a popular and active new theory, established by Mandelbrot in 1977, focusing on random phenomena and irregularities [26]. In 1985, Winslow applied fractal theory to analyze

the pore structure of cement for the first time and reported that the complexity and self-similarity of cement pore structure could be quantitatively characterized using fractal theory [27]. In addition, the fractal theory has been used to analyze the fracture surface and powder morphology of cement-based materials [28]. The fractal dimension is a parameter that quantifies fractal characteristics and can be used to characterize the pore structure, air voids, and fracture surfaces of the mortar and concrete [29]. In order to study the different properties of cementitious composite materials, a series of fractal dimensions have been defined, such as the fractal dimension of the pore surface (D_S), the fractal dimension of the pore volume (D_V), the fractal dimension of the air void (D_a), the fractal dimension of the fracture surface (D_{fs}), and the fractal dimension of the crack (D_C) [30]. D_S is used to characterize the pore surface roughness and pore size distribution, which is usually found by using Neimark's model, Menger sponge model, and Zhang and Li's model [31]. In the above fractal models, Zhang and Li's model is closely related to the principle of the MIP test; therefore, it is more suitable for the fractal analysis of pore structure characteristics and has been widely used. Han et al. reported that the D_S was closely related to the other pore structure parameters such as pore volume and surface area and pore size distribution [32]. Moreover, many studies have shown that the fractal dimension can be used to relate pore structures with macroscopic properties, such as mechanical performance, corrosion resistance, impermeability, and frost resistance [16,26,33]. Therefore, the fractal theory is an effective method to analyze the pore structure of geopolymer composites and its correlation with macroscopic properties.

In summary, many studies have been conducted on MSWIFA geopolymer mortar and the fractal features of geopolymer mortar. However, only a few studies have been conducted on the effect of different contents of MSWIFA on the mechanical properties and pore structure of geopolymer mortars. In addition, the fractal characteristics of pore structures in geopolymer mortars containing MSWIFA and their correlation with compressive strength are rarely investigated. In this study, the compressive strength and pore structure of geopolymer mortar containing MSWIFA were investigated. The pore structure of the mortars was investigated using the pore volume, specific surface area, pore diameter distribution, and fractal characteristics based on mercury intrusion porosimetry (MIP). The D_S of different pore regions of the mortars was calculated by Zhang and Li's model. Additionally, mathematical models of the correlation between the D_S and pore volume, surface area, and compressive strength were established.

2. Materials and Methods

2.1. Materials

MK, FA, and MSWIFA were used as precursors in this study. The SEM images of these precursors are shown in Figure 1. The particle size distribution of these three precursors is shown in Figure 2, measured by Mastersizer 2000 laser (Malvern Instruments Co. LTD., Malvern, UK) particle size analyzer. The volumetric average sizes of MK, FA, and MSWIFA were 4.5 μm, 23.13 μm, and 35.8 μm. Table 1 lists the chemical compositions of these three raw materials as characterized by X-ray fluorescence. The total contents of silica and alumina in MK and FA were 97.83% and 85.45%, whereas little calcium was detected in the MK and FA. On the contrary, the MSWIFA contained up to 35.9% calcium and little silica and alumina. The activating solution was prepared by a sodium silicate solution (SiO_2/Na_2O = 3.2, 34.3% solid content) and sodium hydroxide (99% purity). The modulus (SiO_2/Na_2O) of the alkali activator was adjusted to 1.3 by dissolving the sodium hydroxide in the sodium silicate solution. The fineness modulus of river sand used in this study was 2.7. A superplasticizer with a 25% water-reducing rate was employed to improve the flowability of the geopolymer mortar.

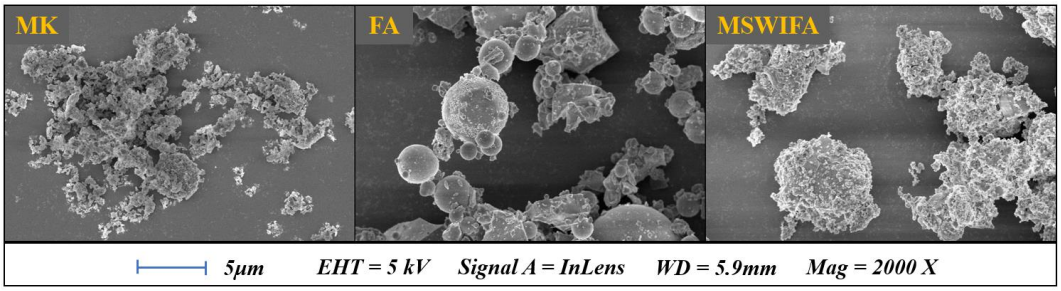

Figure 1. The SEM images of MK, FA, and MSWIFA.

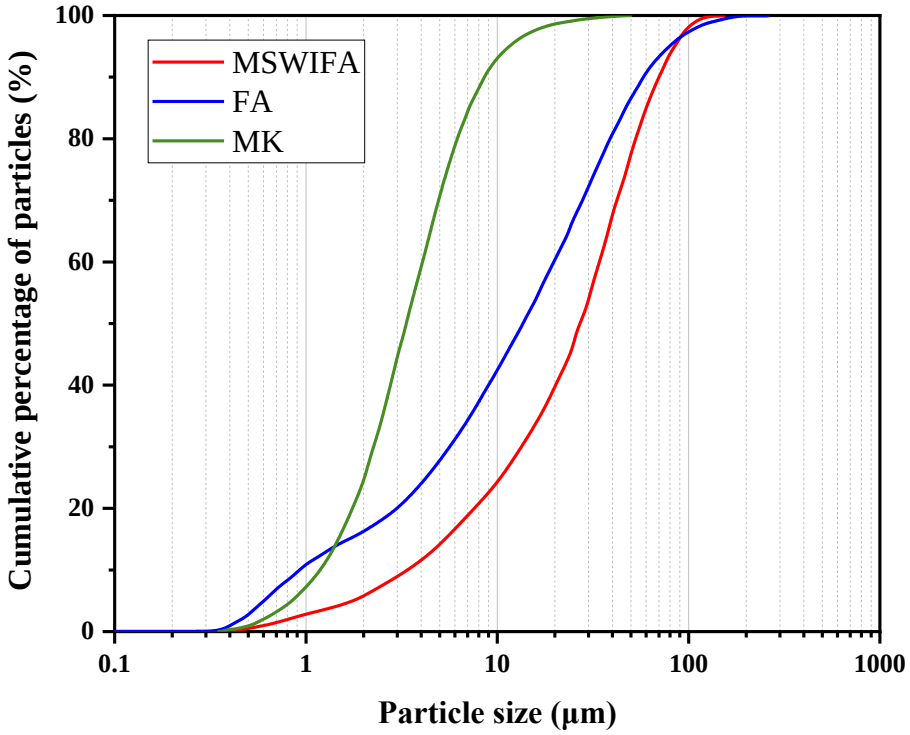

Figure 2. The particle size distribution of MK, FA, and MSWIFA.

Table 1. The chemical compositions of MK, FA, and MSWIFA (wt. %).

Precursors	SiO_2	Al_2O_3	CaO	Fe_2O_3	MgO	K_2O	Na_2O	Cl	LOI
MK	54.31	43.52	0.42	1.17	0.35	0.26	0.18	-	0.50
FA	60.98	24.47	5.58	6.70	0.68	-	-	-	0.75
MSWIFA	3.20	2.70	35.90	0.30	-	9.40	15.40	24.00	12.80

2.2. Synthesis of Geopolymer Mortar

The mix proportions of the geopolymer mortar are summarized in Table 2. The weight content of the MSWIFA in the precursor was 0%, 5%, 15%, 25%, and 35%. The MK was substituted by the MSWIFA with equal weight. The alkali activator was prepared first and stood for 12 h to ensure that the solid sodium hydroxide was completely dissolved. Then, the MK, FA, MSWIFA, and sand were mechanically mixed for 2 min. Afterward, the alkali activator was introduced and mixed for 2 min, and then the superplasticizer and water were poured and mixed for another 2 min. The geopolymer mortar samples were demolded after being cured in the test mold for 24 h. Finally, the samples were cured in a standard curing room (20 °C, 95% relative humidity).

Table 2. The mix proportions of the geopolymer mortars.

Mix ID	FA	MK	MSWIFA	Sand	Na_2SiO_3	NaOH	Water	Superplasticizer
	kg/m^3	kg/m^3	kg/m^3	kg/m^3	kg/m^3	kg/m^3	kg/m^3	%
M-00	355.9	355.9	0	712	446.6	71.9	40.6	1.0
M-05	355.9	320.3	35.8	712	446.6	71.9	40.6	1.0
M-15	355.9	249.1	106.7	712	446.6	71.9	40.6	1.0
M-25	355.9	178.1	178.1	712	446.6	71.9	40.6	1.0
M-35	355.9	106.7	249.1	712	446.6	71.9	40.6	1.0

2.3. Methods

The compressive strength of samples was measured by a microcomputer servo testing machine at a speed of 1.5 kN/s according to the Chinese standard JGJ70-2009. The size of the test specimens was 70.7 × 70.7 × 70.7 mm^3. The MIP test was conducted using a MicroActive AutoPore V 9600 (ATS Scientific, Burlington, ON, Canada). The pore size distribution and pore volume were measured by the cumulative volume and incremental volume of intruded mercury during the compression steps. According to the above tests, the effect of MSWIFA on the compressive strength and pore structure of geopolymer mortar was analyzed. Then, Zhang and Li's model was employed to obtain the surface fractal dimensions of pores in different diameter ranges based on the MIP results. Finally, the relationship of fractal features to other pore structure parameters and compressive strength was investigated.

2.4. Fractal Model

The fractal theory is widely used to analyze the pore characteristics of mortar because it is difficult to characterize the complex pore structure of mortar using only traditional parameters such as pore distribution, pore volume, and specific surface area [31]. Several fractal models have been proposed to calculate the D_S; Zhang and Li's model is a widely used model according to thermodynamics. In the model, the cumulative injection work (W_n) of mercury and the total volume of mercury (V_n) intruded into pores follow the logarithmic law [34,35], as shown in Equation (1).

$$\ln\left(\frac{W_n}{r_n^2}\right) = D_S \ln\left(\frac{V_n^{\frac{1}{3}}}{r_n}\right) + C \tag{1}$$

where r_n and V_n are the pore radius and the volume of the cumulative pore at the n-th mercury intrusion; D_S is the fractal dimension of pore surface; C is a regression constant; and W_n can be determined by Equation (2)

$$W_n = \sum_{i=1}^{n} \overline{P}_i \Delta V_i \tag{2}$$

where i refers to the i-th, whose value ranges from 1 to n; $\overline{P}_i$ is the average pressure of intruded mercury at the stage of i; and ΔV_i is the volume of intruded mercury at the stage of i.

Additionally, if Q_n is defined as Equation (3), Equation (1) would be simplified into Equation (4).

$$Q_n = \frac{V_n^{\frac{1}{3}}}{r_n} \tag{3}$$

$$\ln\left(\frac{W_n}{r_n^2}\right) = D_S \ln(Q_n) + C \tag{4}$$

where Q_n is a function of pore volume V_n and pore radius r_n at the stage n of the mercury intrusion.

The W_n, Q_n, V_n, $\ln\left(\frac{W_n}{r_n^2}\right)$ and $\ln(Q_n)$ can be calculated based on the MIP results and Equations (2) and (3). The D_S is the slope of the fitting line in Equation (4). In this study, D_{SI}, D_{SII}, D_{SIII}, and D_{SIV} were defined and corresponded to the surface fractal dimensions of pores with the diameter ranges of <20 nm, 20–50 nm, 50–200 nm, and >200 nm.

3. Results and Discussion

3.1. Compressive Strength

The compressive strength of geopolymer mortars with different contents of MSWIFA is shown in Figure 3. The compressive strength of the mortars decreases with the increase in MSWIFA content. The compressive strength of geopolymer mortar decreases by 24.7%, 52.2%, 58.3%, and 77.6% at 5%, 15%, 25%, and 35% MSWIFA content. Casanova et al. also reported that the MSWIFA decreased the strength of geopolymer mortar [36]. The decrease in compressive strength in geopolymer mortars is mainly due to three reasons. Firstly, the calcium silicate aluminate (C-A-S-H) and sodium silicate aluminate (N-A-S-H) mainly provide the strength of the samples [37]. The MK, which was partially replaced by MSWIFA, contains 97% SiO_2 and Al_2O_3. However, the total content of SiO_2 and Al_2O_3 in the MSWIFA only accounts for 4%. Therefore, with the increase in MSWIFA content, the amount of N-A-S-H and C-A-S-H gels decreased, resulting in a decrease in the compressive strength of the geopolymer mortar. Secondly, the high specific surface area and low activity of MSWIFA led to excess water adsorbing on the surface of MSWIFA that would not participate in subsequent hydration reactions [19]. Consequently, the excess water evaporated gradually, resulting in an increase in porosity and adversely affecting the strength of geopolymer mortar [38]. Thirdly, the presence of chloride ions in the MSWIFA could deteriorate the internal structure and reduce the strength of the mortar [39]. However, several researchers reported that the compressive strength of geopolymer mortars increased first and then decreased with the increment in MSWIFA content [22,38]. This was because the MSWIFA used in their studies contained more active substances (CaO and SiO_2) compared with that used in this study. Therefore, the MSWIFA provided from various sources shows different compositions and properties.

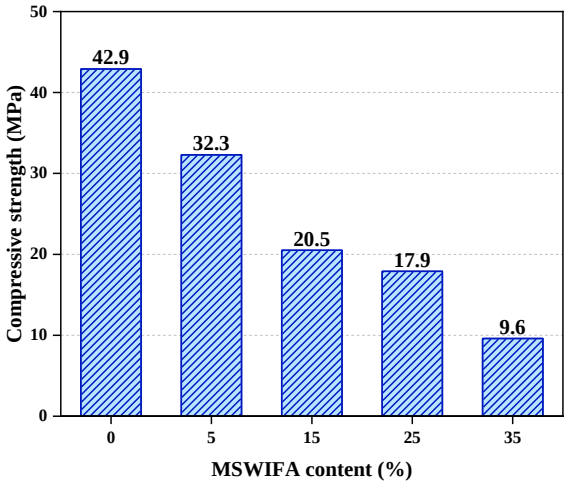

Figure 3. The compressive strength of geopolymer mortars.

3.2. Pore Diameter Distribution

The incremental and cumulative pore volumes of geopolymer mortars are shown in Figure 4. The pressure range of mercury intrusion was 0.5–33,000 psia (0.0034–228 MPa), corresponding to a pore diameter of 5.48 nm–355 µm. According to Figure 4a, the incremental pore volume curves of mortars containing different MSWFIFA contents exhibit similar contours. At 5–50 nm of pore diameter, the highest peaks of incremental pore volume curves can be observed, indicating that the most probable pore diameters of mortars are

between 5 and 50 nm. Additionally, it can be seen that the increased pore volume at the 500–5000 nm diameter range increases with the MSWIFA content. When the pore diameter exceeds 5000 nm, even though the contours of curves are not uniform, it can still be observed that the MSWIFA increases the pore volume of the geopolymer mortar. This is because using MSWIFA instead of MK reduced the hydration products available to fill pores, resulting in an increase in the pore volume. Moreover, the MSWIFA brought more adsorbed water, whose evaporation created pores. Therefore, the use of MSWIFA led to an increase in pore volume for almost all pore sizes in the tested range. Long et al. also reported that the decrease in MSWIFA content significantly reduced the volume of pores larger than 20 nm [40].

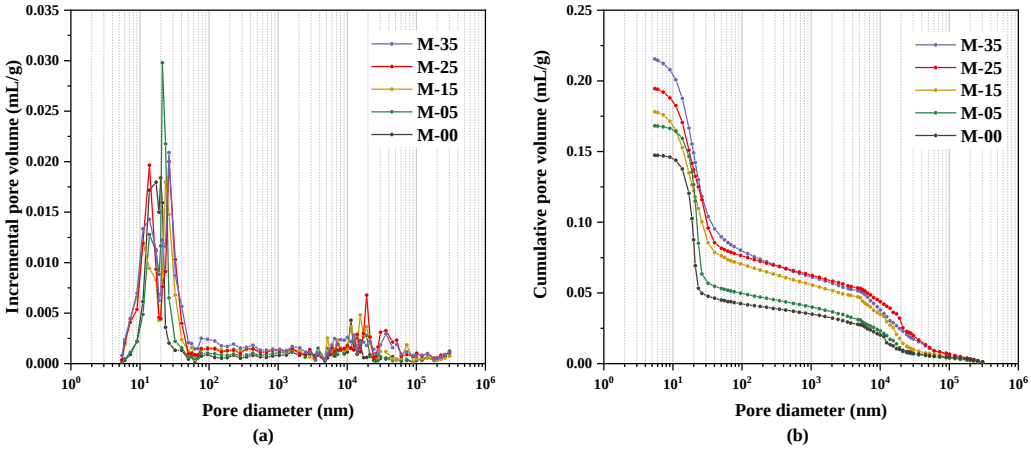

Figure 4. The incremental pore volume (**a**) and cumulative pore volume (**b**) of geopolymer mortars.

Five cumulative pore volume curves with similar shapes are shown in Figure 4b. The cumulative pore volume curves move up with the increase in MSWIFFA content, indicating that the pore volume in geopolymer mortar increases as the MSWIFA content increases. The threshold pore diameter is the pore diameter corresponding to the junction of the slow and fast-rising part of the cumulative pore volume curve. The applied intrusion pressure would increase significantly when the mercury intruded into pores with the threshold diameter, and the pore volume obviously increased at the same time. The threshold pore diameter of mortars increased with the MSWIFA content. This indicates that the MSWIFA increased the overall pore size in the mortars, which corresponds to the incremental pore volume result. Bai et al. also reported that the addition of MSWIFA would produce soluble salt and inhibit the hydration process, which increased porosity and loosened microstructure [38].

3.3. Pore Volume and Specific Surface Area Distribution

The pore morphology in the mortar is diverse, including open pores, ink-bottle pores, closed pores, and open-ended pores [41,42]. In addition, the diameter of pores ranges from nanometers to centimeters. The distribution of pores with different sizes and shapes in mortar is irregular. Pores with different sizes show various effects on the properties of the mortar. Therefore, researchers often divide pores into several regions based on the pore diameter. However, there is no consensus on the classification criteria of pores. To analyze the relationship between the strength and pore structure of the geopolymer mortar, the pores were classified into harmless pores (<20 nm), slightly harmful pores (20–50 nm), harmful pores (50–200 nm), and very harmful pores (>200 nm). Figure 5 indicates the pore volume distribution of geopolymer mortars. As the MSWIFA content increases, the total pore volume increases. The volume of slightly harmful, harmful, and very harmful pores increases but the harmless pore volume decreases as the MSWIFA content increases. Combined with the compressive strength of mortars, the increase in slightly harmful, harmful, and very harmful pores volumes decreased the strength of geopolymer mortar, and the reduction in harmless pore volume did not result in an

increase in strength. Bai et al. [38] and Long et al. [40] also observed that the volume of pores (<30 nm) decreased while the pore volume in the range of 30–2000 nm increased with the MSWIFA content. As seen in Figure 4, the pore volume from 5 to 10 nm (gel pores) increases but the pore volume in the range of 10–20 nm decreases with the increase in MSWIFA content. This is probably because the addition of MSWIFA increased the CaO content, which accelerated the hydration reaction and refined the pores [37]. However, the decrease in the SiO_2 and Al_2O_3 content reduced the formation of N (C) -A-S-H generation, which reduced the gel accumulation and increased the gel pores.

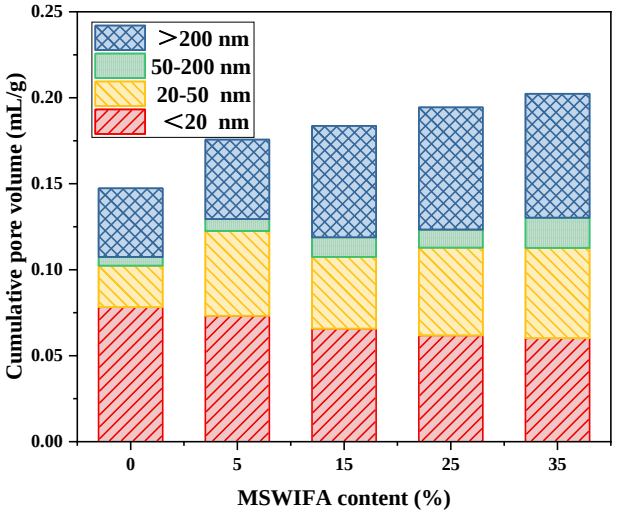

Figure 5. The pore volume distribution of geopolymer mortars.

Figure 6 shows the specific surface area of the various types of pores. The total specific surface area of geopolymer mortar increases with the MSWIFA content, which corresponds to the increase in total pore volume. The harmless and slightly harmful pores provide most of the surface area. This indicates that the micropores mainly determine the specific surface area of geopolymer mortar. Previous studies also reported that the micropores determined the specific surface area [31]. This is because the specific surface area is calculated by the pore diameter and pore volume. It is worth noting that the specific surface area of harmless pores increased, while the volume decreased as the MSWIFA content increased. This was due to the refinement of harmless pores, meaning that the number of 5–10 nm pores increased while the number of 10–20 nm pores decreased.

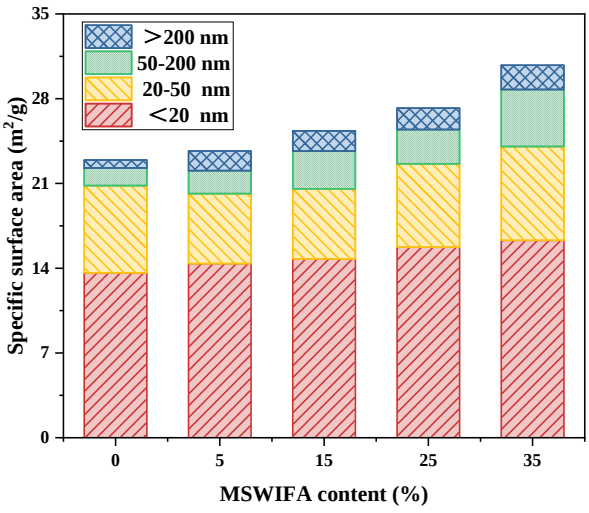

Figure 6. The specific surface area distribution of geopolymer mortars.

3.4. Fractal Dimension Analysis

Based on the harmful degree of pores, four segments of pores were divided, namely, Region I (<20 nm), Region II (20–50 nm), Region III (50–200 nm), and Region IV (>200 nm). The regression lines of different regions for mortars are shown in Figure 7, and the D_S values are listed in Table 3. The surface fractal dimension shows a scale-dependent property. According to previous studies, the scale-dependent property is a familiar property of the pore fractal in mortar and concrete, owing to the diversity of pore morphology and irregularity of pore distribution [26,43]. Pores in Region I and Region IV present significant fractal characteristics. Both the D_{SI} and D_{SIV} values are between 2 and 3, indicating that the pores of these two regions are rough. Based on the fractal theory, if the pore surface is completely smooth, the D_S will be equal to 2, and the pore surface becomes rougher as the D_S approaches 3. When the D_S exceeds 3, it is considered nonphysical and the surface fractal dimension value is invalid [28]. The D_S of Region II and III is higher than 3 in this study. Previous studies have also shown the "nonphysical" aspect of the surface fractal dimensions in transition regions [31,32]. This may be because the assumptions of MIP are too idealistic. All the pores in the specimen are assumed to be open in the MIP test. However, semi-open pores and closed pores in the mortar could not be detected. In addition, the MIP is calculated according to the cylindrical pore model, whereas the pore morphology in the sample is diverse. The ink bottle pores are often considered the main reason for the non-fractal regions [41]. The inlet of the ink bottle pore is smaller than its inner diameter, resulting in mercury hysteresis. The measured diameter is smaller than the real diameter of the ink bottle hole; therefore, small pore numbers are overestimated and large pore numbers are underestimated. Previous studies also reported the non-fractal phenomenon and its reason [33,44].

The D_{SI} values of mortars are between 2.781 to 2.735. The pores in Region I are related to the interlayer structure of hydration products and the microstructure of each phase. Pores with a diameter smaller than 20 nm are considered harmless to the strength and therefore are namely harmless pores. However, they are thought to have a great effect on the creep and shrinkage of samples [41]. Furthermore, the degree of hydration and microstructure compactness can be speculated based on the pores in Region I. As shown in Figure 7 and Table 3, the D_{SI} decreases with the increase in MSWIFA content, indicating that the addition of MSWIFA reduces the roughness and complexity of pores in Region I. This is because the substitution of MK with MSWIFA reduced the formation of N (C)-A-S-H gel, resulting in less accumulation of gels. Therefore, the complexity and roughness of pores decreased with the increase in MSWIFA content.

The D_{SIV} values range from 2.762 to 2.724 can be seen in Figure 7 and Table 3. The pores in the Region IV of >200 nm correspond to the capillary pores between hydration product particles, and the air voids entrained in the geopolymer mortar. Previous studies showed that although the evenly distributed pores could improve the frost resistance of the mortar, the large pores exhibited a negative effect on strength and permeability [28]. The D_{SIV} also decreased as the MSWIFA content increased in this study. This indicated that the admixture of MSWIFA reduced the complexity and roughness of pores in Region IV; probably because the addition of MSWIFA limited the hydration, which reduced the amount of hydration product. Consequently, the compactness of hydration particle accumulation decreased, resulting in an increase in pore volume and a decrease in the complexity of pores. It is worth noting that the D_{SI} is always greater than D_{SIV}, suggesting that the pores in Region I are more complex than that in Region IV.

Generally, the internal characteristics and spatial distribution of pores in mortar can be well described by fractal curves and fractal dimensions. However, both scale-dependency and self-similarity of pore surface for mortar only exist in certain ranges. Therefore, reasonable ranges of pore diameter should be chosen to analyze the pore structure when the test method is MIP. The following analysis in this study mainly focuses on the pores in Region I and Region IV.

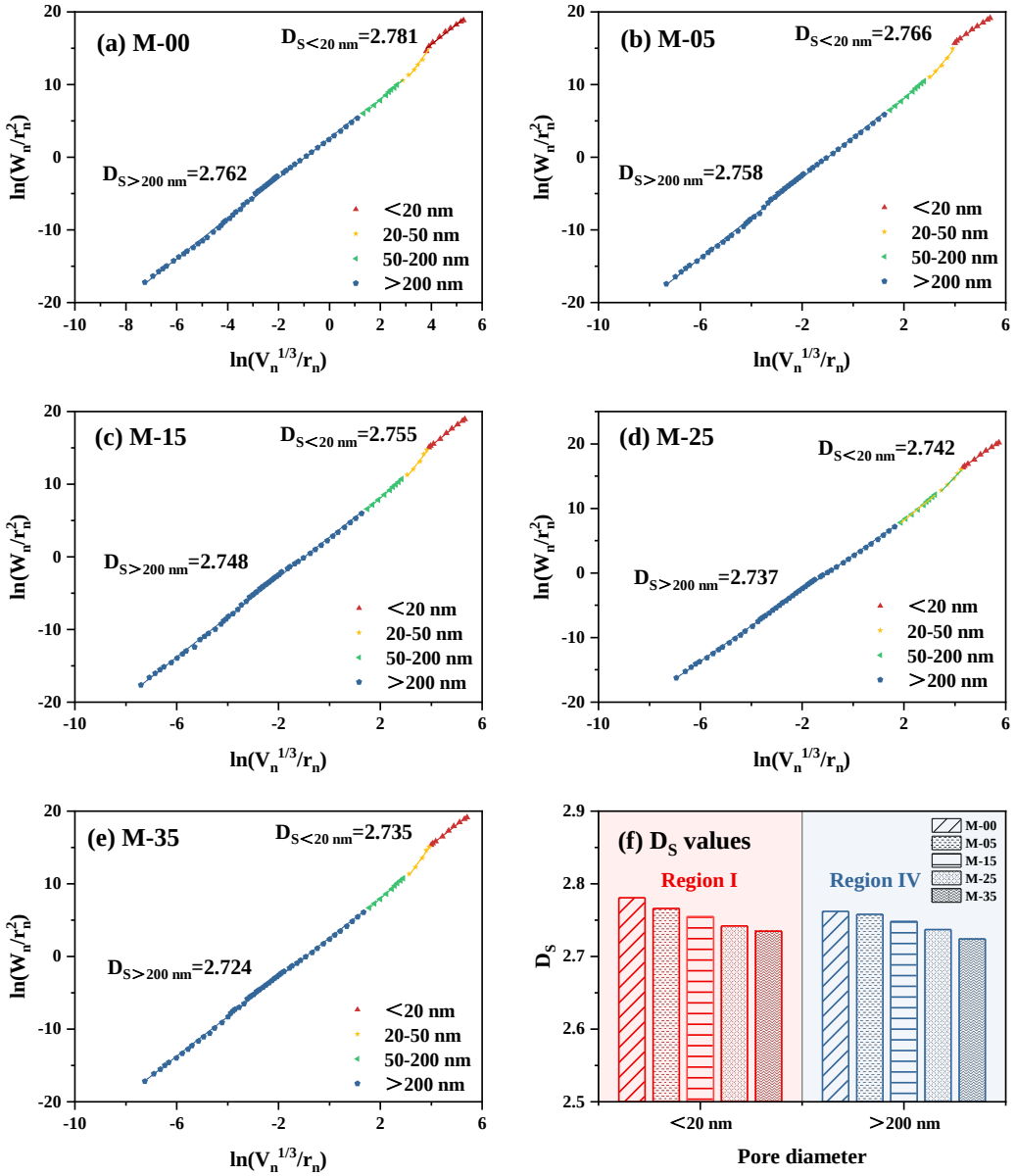

Figure 7. $\ln\left(W_n/r_n^2\right)$ vs. $\ln\left(V_n^{1/3}/r_n\right)$ and the D_S values in the mortars: (**a**) M-00, (**b**) M-05, (**c**) M-15, (**d**) M-25, (**e**) M-35, and (**f**) the D_S values in Region I and Region IV of mortars.

Table 3. The D_S of geopolymer mortars.

Mortars	Region I	Region II	Region III	Region IV
M-00	2.781	4.796	3.006	2.762
M-05	2.766	4.623	3.039	2.758
M-15	2.755	4.453	3.073	2.748
M-25	2.742	4.242	3.132	2.737
M-35	2.735	4.114	3.2	2.724

3.5. Correlation between Pore Structure Features and Fractal Dimension

To characterize the pore structure of mortar, many parameters are used, such as pore volume, specific surface area, porosity, and pore size distribution. None of these parameters can accurately describe the pore structure. Some of these parameters can be calculated using other parameters, for example, the porosity and average pore size can be calculated by the pore surface area and pore volume. Both the pore volume and pore surface area can

be regarded as fractal objects. The relationships between the fractal dimension and specific surface area and pore volume in Region I and Region IV are investigated because the pore structure shows the fractal feature only in these two regions. The relationship between the pore volume and fractal dimension is shown in Figure 7a,b. There is a positive correlation between pore volume and D_{SI} but a negative correlation between pore volume and D_{SIV}. The correlation coefficients of Region I and Region IV are 0.969 and 0.835, respectively, indicating a good correlation between the pore volume and fractal dimension. The links between the specific surface area and fractal dimension of Region I and Region IV are shown in Figure 8c,d, showing a negative correlation in both regions. The correlation coefficient in Region IV is less than that of Region I because the formation mode of pores in different regions of mortar is different, leading to multifractal characteristics.

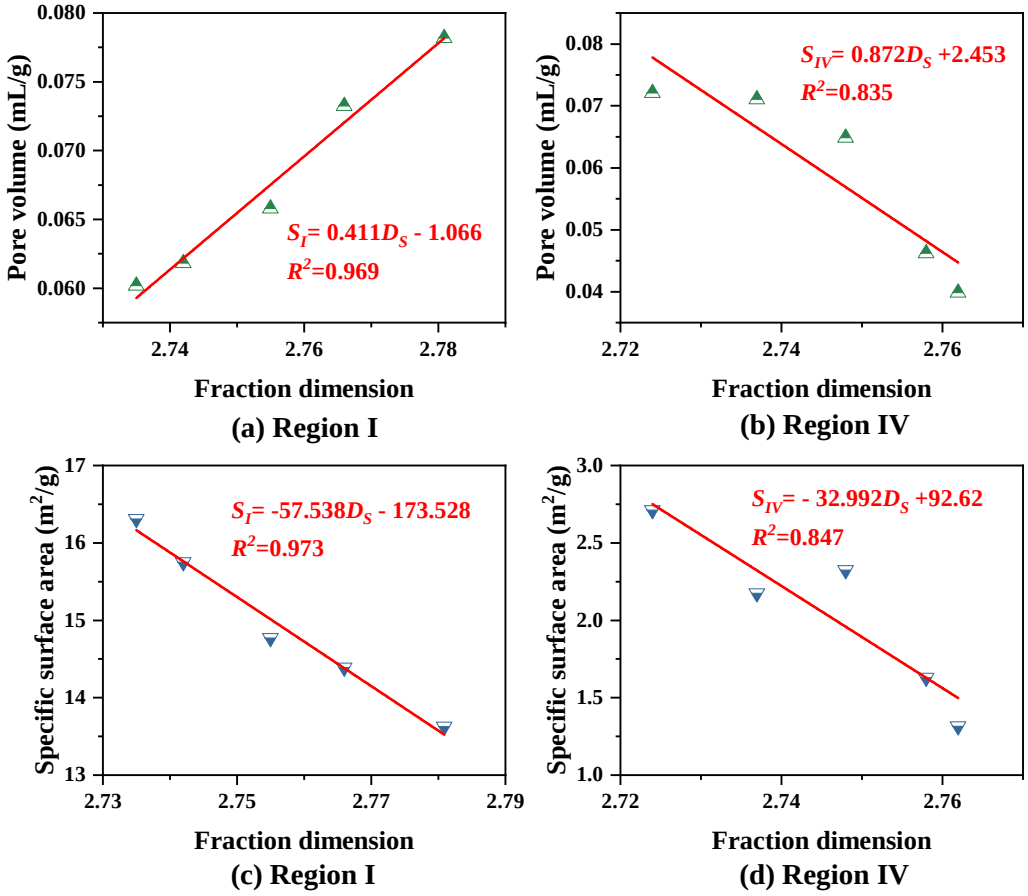

Figure 8. The correlation between fractal dimension and (**a**,**b**) pore volume and (**c**,**d**) specific surface area.

According to the relationship between D_{SI} and specific surface area and pore volume, the surface area increases while the pore volume decreases with the decrease in D_{SI}. This was because the increase in MSWIFA content led to the refinement of the pores in Region I, meaning that the volume of larger pores (10–20 nm) decreased, while the volume of smaller pores (<10 nm) increased. The increase in the proportion of smaller pores (<10 nm) caused an increase in specific surface area and a decrease in the pore volume. Additionally, the refinement of pores resulted in an increase in the pore roughness in Region I and an increase in the D_{SI}, which is consistent with the fractal theory. The D_{SIV} is negatively correlated with both the specific surface area and pore volume as shown in Figure 8. This was because the specific surface area and pore volume increased with the MSWIFA content. The complexity and roughness of pores in Region IV decreased, resulting in a decrease in the D_{SIV}. In general, the pore structure characteristics of geopolymer mortar containing MSWIFA can be clearly described by fractal dimension. Furthermore, the specific surface

area and pore volume show a good relationship with the fractal dimension. Therefore, they can be deduced by the fractal dimension.

3.6. Correlation between Compressive Strength and Fractal Dimension

Many studies have reported that the strength of porous gel materials is dependent on the pore structure and the mathematical models between strength and pore structure have been established [26,41]. However, the mathematical model will be too complex if all of the pore structure parameters are considered. Therefore, it is necessary to use a representative pore structure parameter in order to ensure the simplicity and accuracy of the mathematical model. According to the analysis in Section 3.5, the fractal dimension of pores is a comprehensive parameter that can reflect the spatial distribution and morphology of pores. Hence, the fractal dimension was used to predict the compressive strength of the geopolymer mortar in this study. As shown in Figure 9, the compressive strength of samples is linearly correlated with the fractal dimension. The correlation coefficients between the compressive strength and D_{SI} and D_{SIV} are 0.956 and 0.893, respectively. The compressive strength increases with the D_{SI} and D_{SIV}.

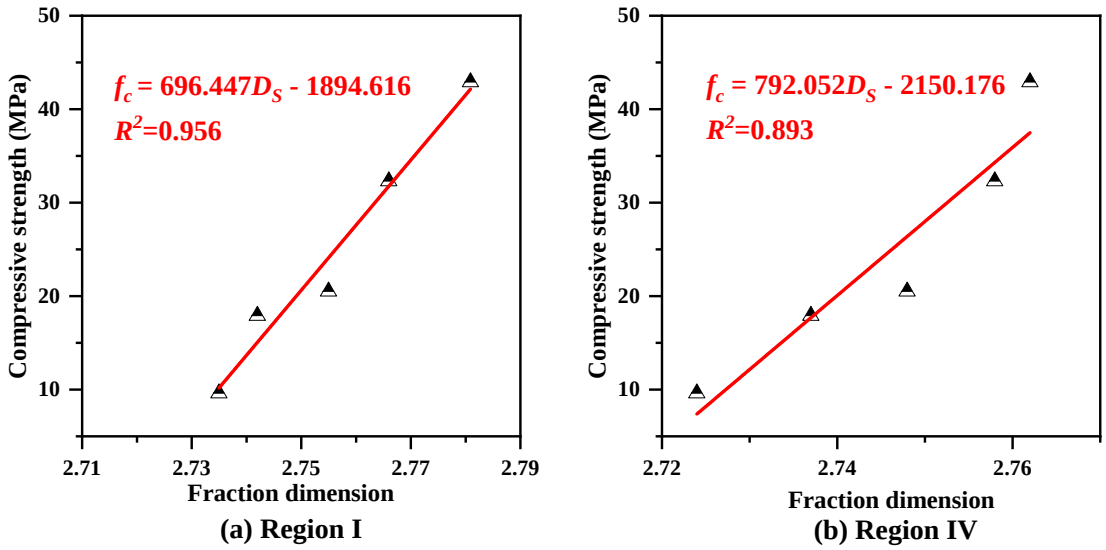

Figure 9. The relationship between compressive strength and fractal dimension.

The pore with a large fractal dimension has a complex pore structure, meaning a stable accumulation mode of hydration products. Therefore, the amount and compactness of the hydration product decreased with the increase in MSWIFA content, resulting in a decrease in D_{SI} and D_{SIV} and the compressive strength of the geopolymer mortars. It is reported that large pores have a greater effect on compressive strength than small pores [45]. Consequently, the compressive strength of mortars increased with the D_{SIV}. The pores in Region I are considered harmless pores, while the D_{SI} reflects the degree of hydration and the pattern of gel accumulation. Therefore, the D_{SI} is also positively correlated with compressive strength. Han et al. also reported that the surface fractal dimensions in Region I and Region IV showed a positive correlation with compressive strength [32]. However, contrary to the report by Han et al., the correlation coefficient in Region IV is even smaller than that in Region I in this study. This is probably because the addition of MSWIFA increased the irregularity of pore distribution in Region IV.

Overall, the mathematical model in Figure 9 well expresses the relationship between the macroscopic compressive strength and microscopic pore structure of geopolymer mortars. In contrast, the D_{SI} has a better correlation with compressive strength. Therefore, the model in Region I is a better choice to predict the compressive strength of the geopolymer mortar containing MSWIFA.

4. Conclusions

In this study, compression and MIP tests were used to analyze the effect of MSWIFA content on the compressive strength and pore structure of geopolymer mortar. The pore structure features and fractal dimension based on Zhang and Li's model were investigated. Additionally, the correlations between the fractal dimension and compressive strength and pore structure were considered. The following conclusions were drawn:

(1) The compressive strength decreases with the increase in the MSWIFA content in the geopolymer mortar. When the MSWIFA content was 35%, the compressive strength of the mortar decreased by 77.6%. The addition of MSWIFA increases the overall pore size in the mortar. The total specific surface area and pore volume of the mortars increase with the increase in MSWIFA content.

(2) The addition of MSWIFA causes an increase in the specific surface area and pore volume for the slightly harmful, harmful, and very harmful pores. As the MSWIFA content increases, the decrease in the specific surface area and the increase in the pore volume of the harmless pores suggests the refinement of the harmless pores. Specifically, the number of pores in the 5–10 nm range increases but the number of pores in the 10–20 nm range decreases with the increase in the MSWIFA content.

(3) The D_{SI} values of mortars are between 2.788 to 2.719 and the D_{SIV} ranges from 2.708 to 2.766, indicating the obvious fractal characteristics in Regions I and IV. However, some pores do not conform to fractal characteristics because the pore morphology is different from the hypothetical pore model. The D_{SII} and D_{SIII} exceed 3, which means that the pores in Regions II and III are non-physical according to the surface geometry. The complexity of pores in Regions I and IV decreases with the increase in the MSWIFA content, and the pores in Region I always show a more complex structure than that in Region IV.

(4) The fractal dimension exhibits a good relationship with the specific surface area and pore volume. The D is a comprehensive parameter that can reflect the morphology and the pore spatial distribution in geopolymer mortars. The D_{SI} and D_{SIV} are linearly related to the compressive strength of the geopolymer mortar, and the correlations are good. Therefore, the pore surface fractal dimension of geopolymer mortar containing MSWIFA can be used to predict the specific surface area, pore volume, and compressive strength.

Author Contributions: Data curation, X.H.; Formal analysis, P.Z. and X.H.; Funding acquisition, P.Z.; Investigation, P.Z., X.H. and J.G.; Methodology, X.H. and H.Z.; Project administration, J.G.; Resources, J.G.; Validation, H.Z.; Visualization, P.Z.; Writing—Original draft, P.Z.; Writing—Review and editing, X.H., J.G. and H.Z.; All authors have read and agreed to the published version of the manuscript.

Funding: This research was funded by the National Natural Science Foundation of China (Grant No. 52278283, U2040224), Natural Science Foundation of Henan of China (Grant No. 212300410018), and Project Special Funding of Yellow River Laboratory (Grant No. YRL22LT02).

Data Availability Statement: The data that support the findings of this study are available from the corresponding author upon reasonable request.

Acknowledgments: The authors would like to thank all the anonymous reviewers for their constructive comments and suggestions.

Conflicts of Interest: The authors declare no conflict of interest.

References

1. Wen, C.; Zhang, P.; Wang, J.; Hu, S. Influence of fibers on the mechanical properties and durability of ultra-high-performance concrete: A review. *J. Build. Eng.* **2022**, *52*, 104370. [CrossRef]
2. Zhang, P.; Wei, S.; Zheng, Y.; Wang, F. Effect of single and synergistic reinforcement of PVA fiber and nano-SiO_2 on workability and compressive strength of geopolymer composites. *Polymers* **2022**, *14*, 3765. [CrossRef] [PubMed]
3. Ranjbar, N.; Kuenzel, C.; Spangenberg, J.; Mehrali, M. Hardening evolution of geopolymers from setting to equilibrium: A review. *Cem. Concr. Compos.* **2020**, *114*, 103729. [CrossRef]

4. Zhang, P.; Kang, L.; Zheng, Y.; Zhang, T.; Zhang, B. Influence of SiO_2/Na_2O molar ratio on mechanical properties and durability of metakaolin-fly ash blend alkali-activated sustainable mortar incorporating manufactured sand. *J. Mater. Res. Technol.* **2022**, *18*, 3553–3563. [CrossRef]
5. Zhang, P.; Gao, Z.; Wang, J.; Guo, J.; Wang, T. Influencing factors analysis and optimized prediction model for rheology and flowability of nano-SiO_2 and PVA fiber reinforced alkali-activated composites. *J. Clean. Prod.* **2022**, *366*, 132988. [CrossRef]
6. Guo, X.; Yang, J.; Xiong, G. Influence of supplementary cementitious materials on rheological properties of 3D printed fly ash based geopolymer. *Cem. Concr. Compos.* **2020**, *114*, 103820. [CrossRef]
7. Zhang, P.; Han, X.; Hu, S.; Wang, J.; Wang, T. High-temperature behavior of polyvinyl alcohol fiber-reinforced metakaolin/fly ash-based geopolymer mortar. *Compos. B Eng.* **2022**, *244*, 110171. [CrossRef]
8. Han, Q.; Zhang, P.; Wu, J.; Jing, Y.; Zhang, D.; Zhang, T. Comprehensive review of the properties of fly ash-based geopolymer with additive of nano-SiO_2. *Nanotechnol. Rev.* **2022**, *11*, 1478–1498. [CrossRef]
9. Rivera, O.G.; Long, W.R.; Weiss, C.A., Jr.; Moser, R.D.; Williams, B.A.; Torres-Cancel, K.; Gore, E.R.; Allison, P.G. Effect of elevated temperature on alkali-activated geopolymeric binders compared to portland cement-based binders. *Cem. Concr. Res.* **2016**, *90*, 43–51. [CrossRef]
10. Guo, X.; Xiong, G. Resistance of fiber-reinforced fly ash-steel slag based geopolymer mortar to sulfate attack and drying-wetting cycles. *Constr. Build. Mater.* **2021**, *269*, 121326. [CrossRef]
11. Jin, Q.; Zhang, P.; Wu, J.; Sha, D. Mechanical properties of nano-SiO_2 reinforced geopolymer concrete under the coupling effect of a wet-thermal and chloride salt environment. *Polymers* **2022**, *14*, 2298. [CrossRef] [PubMed]
12. Sun, Z.; Vollpracht, A.; van der Sloot, H.A. pH dependent leaching characterization of major and trace elements from fly ash and metakaolin geopolymers. *Cem. Concr. Res.* **2019**, *125*, 105889. [CrossRef]
13. Korniejenko, K.; Kejzlar, P.; Louda, P. The influence of the material structure on the mechanical properties of geopolymer composites reinforced with short fibers obtained with additive technologies. *Int. J. Mol. Sci.* **2022**, *23*, 2023. [CrossRef]
14. Ponsot, I.; Bernardo, E.; Bontempi, E.; Depero, L.; Detsch, R.; Chinnam, R.K.; Boccaccini, A.R. Recycling of pre-stabilized municipal waste incinerator fly ash and soda-lime glass into sintered glass-ceramics. *J. Clean. Prod.* **2015**, *89*, 224–230. [CrossRef]
15. Niu, M.; Zhang, P.; Guo, J.; Wang, J. Effect of municipal solid waste incineration fly ash on the mechanical properties and microstructure of geopolymer concrete. *Gels* **2022**, *8*, 341. [CrossRef] [PubMed]
16. Wang, L.; Yu, Z.; Liu, B.; Zhao, F.; Tang, S.; Jin, M. Effects of fly ash dosage on shrinkage, crack resistance and fractal characteristics of face slab concrete. *Fractal. Fract.* **2022**, *6*, 335. [CrossRef]
17. Tian, X.; Rao, F.; León-Patiño, C.A.; Song, S. Co-disposal of MSWI fly ash and spent caustic through alkaline-activation: Immobilization of heavy metals and organics. *Cem. Concr. Compos.* **2020**, *114*, 103824. [CrossRef]
18. Carvalho, R.; Silva, R.V.; de Brito, J.; Pereira, M.F.C. Alkali activation of bottom ash from municipal solid waste incineration: Optimization of NaOH- and Na_2SiO_3-based activators. *J. Clean. Prod.* **2021**, *291*, 125930. [CrossRef]
19. Kan, L.; Shi, R.; Zhao, Y.; Duan, X.; Wu, M. Feasibility study on using incineration fly ash from municipal solid waste to develop high ductile alkali-activated composites. *J. Clean. Prod.* **2020**, *254*, 120168. [CrossRef]
20. Zhu, W.; Rao, X.H.; Liu, Y.; Yang, E.-H. Lightweight aerated metakaolin-based geopolymer incorporating municipal solid waste incineration bottom ash as gas-forming agent. *J. Clean. Prod.* **2018**, *177*, 775–781. [CrossRef]
21. Kan, L.; Wang, F. Mechanical properties of high ductile alkali-activated fiber reinforced composites incorporating red mud under different curing conditions. *Ceram. Int.* **2022**, *48*, 1999–2011. [CrossRef]
22. Fan, C.; Wang, B.; Ai, H.; Qi, Y.; Liu, Z. A comparative study on solidification/stabilization characteristics of coal fly ash-based geopolymer and Portland cement on heavy metals in MSWI fly ash. *J. Clean. Prod.* **2021**, *319*, 128790. [CrossRef]
23. Zheng, Y.; Zhuo, J.; Zhang, P.; Ma, M. Mechanical properties and meso-microscopic mechanism of basalt fiber-reinforced recycled aggregate concrete. *J. Clean. Prod.* **2022**, *370*, 133555. [CrossRef]
24. Wang, L.; Li, G.; Li, X.; Guo, F.; Tang, S.; Lu, X.; Hanif, A. Influence of reactivity and dosage of MgO expansive agent on shrinkage and crack resistance of face slab concrete. *Cem. Concr. Compos.* **2022**, *126*, 104333. [CrossRef]
25. Yang, H.M.; Zhang, S.M.; Wang, L.; Chen, P.; Shao, D.K.; Tang, S.W.; Li, J.Z. High-ferrite Portland cement with slag: Hydration, microstructure, and resistance to sulfate attack at elevated temperature. *Cem. Concr. Compos.* **2022**, *130*, 104560. [CrossRef]
26. Peng, Y.; Tang, S.; Huang, J.; Tang, C.; Liu, Y. Fractal analysis on pore structure and modeling of hydration of magnesium phosphate cement paste. *Fractal Fract.* **2022**, *6*, 337. [CrossRef]
27. Yang, J.; Huang, J.; He, X.; Su, Y.; Tan, H.; Chen, W.; Wang, X.; Strnadel, B. Segmented fractal pore structure covering nano- and micro-ranges in cementing composites produced with GGBS. *Constr. Build. Mater.* **2019**, *225*, 1170–1182. [CrossRef]
28. Lan, X.-L.; Zeng, X.-H.; Zhu, H.-S.; Long, G.-C.; Xie, Y.-J. Experimental investigation on fractal characteristics of pores in air-entrained concrete at low atmospheric pressure. *Cem. Concr. Compos.* **2022**, *130*, 104509. [CrossRef]
29. Kan, L.; Wang, F.; Zhang, Z.; Kabala, W.; Zhao, Y. Mechanical properties of high ductile alkali-activated fiber reinforced composites with different curing ages. *Constr. Build. Mater.* **2021**, *306*, 124833. [CrossRef]
30. Gao, Y.; Wu, K.; Yuan, Q. Limited fractal behavior in cement paste upon mercury intrusion porosimetry test: Analysis and models. *Constr. Build. Mater.* **2021**, *276*, 122231. [CrossRef]
31. Li, D.; Niu, D.; Fu, Q.; Luo, D. Fractal characteristics of pore structure of hybrid Basalt–Polypropylene fibre-reinforced concrete. *Cem. Concr. Compos.* **2020**, *109*, 103555. [CrossRef]

32. Han, X.; Wang, B.; Feng, J. Relationship between fractal feature and compressive strength of concrete based on MIP. *Constr. Build. Mater.* **2022**, *322*, 126504. [CrossRef]
33. Wang, L.; Zeng, X.; Yang, H.; Lv, X.; Guo, F.; Shi, Y.; Hanif, A. Investigation and application of fractal theory in cement-based materials: A review. *Fractal Fract.* **2021**, *5*, 247. [CrossRef]
34. Zhang, B.; Li, S. Determination of the surface fractal dimension for porous media by mercury porosimetry. *Ind. Eng. Chem. Res.* **1995**, *34*, 1383–1386. [CrossRef]
35. Zhang, B.; Liu, W.; Liu, X. Scale-dependent nature of the surface fractal dimension for bi- and multi-disperse porous solids by mercury porosimetry. *Appl. Surf. Sci.* **2006**, *253*, 1349–1355. [CrossRef]
36. Casanova, S.; Silva, R.V.; de Brito, J.; Pereira, M.F.C. Mortars with alkali-activated municipal solid waste incinerator bottom ash and fine recycled aggregates. *J. Clean. Prod.* **2021**, *289*, 125707. [CrossRef]
37. Tian, X.; Rao, F.; León-Patiño, C.A.; Song, S. Co-disposal of MSWI fly ash and spent caustic through alkaline-activation consolidation. *Cem. Concr. Compos.* **2021**, *116*, 103888. [CrossRef]
38. Bai, Y.; Guo, W.; Wang, X.; Pan, H.; Zhao, Q.; Wang, D. Utilization of municipal solid waste incineration fly ash with red mud-carbide slag for eco-friendly geopolymer preparation. *J. Clean. Prod.* **2022**, *340*, 130820. [CrossRef]
39. Chen, L.; Wang, L.; Cho, D.-W.; Tsang, D.C.W.; Tong, L.; Zhou, Y.; Yang, J.; Hu, Q.; Poon, C.S. Sustainable stabilization/solidification of municipal solid waste incinerator fly ash by incorporation of green materials. *J. Clean. Prod.* **2019**, *222*, 335–343. [CrossRef]
40. Long, W.; Peng, J.; Gu, Y.; Li, J.; Dong, B.; Xing, F.; Fang, Y. Recycled use of municipal solid waste incinerator fly ash and ferronickel slag for eco-friendly mortar through geopolymer technology. *J. Clean. Prod.* **2021**, *307*, 127281. [CrossRef]
41. Hong, G.; Oh, S.; Kim, J.; Chin, W.-J.; Kim, Y.-J.; Choi, S.; Song, C. Surface-fractal-dimension characteristics of cementitious composites with multi-walled carbon nanotubes dispersed by silica fume. *Constr. Build. Mater.* **2022**, *329*, 127182. [CrossRef]
42. Wang, L.; Huang, Y.; Zhao, F.; Huo, T.; Chen, E.; Tang, S. Comparison between the influence of finely ground phosphorous slag and fly ash on frost resistance, pore structures and fractal features of hydraulic concrete. *Fractal Fract.* **2022**, *6*, 598. [CrossRef]
43. Zhao, D.; Guo, Y.; Wang, G.; Guan, X.; Zhou, X.; Liu, J. Fractal analysis and classification of pore structures of high-rank coal in Qinshui Basin, China. *Energies* **2022**, *15*, 6766. [CrossRef]
44. Zhang, P.; Wang, K.; Wang, J.; Guo, J.; Ling, Y. Macroscopic and microscopic analyses on mechanical performance of metakaolin/fly ash based geopolymer mortar. *J. Clean. Prod.* **2021**, *294*, 126193. [CrossRef]
45. Wang, K.; Guo, J.; Liu, X.; Yang, L.; Zhang, P. Effect of dry–wet ratio on pore-structure characteristics of fly ash concrete under sulfate attack. *Mater. Struct.* **2021**, *54*, 100. [CrossRef]